 CMES, vol.69, no.2, pp.91-117, 2010

MLPG Application of Nanofluid Flow Mixed Convection Heat Transfer in a Wavy Wall Cavity

A. Arefmanesh[1], M. Najafi[2] and M. Nikfar[3]

Abstract: Procuring a numerical solution through an application of the meshless local Petrov-Galerkin method (MLPG) on the fluid flow and mixed convection in a complex geometry cavity filled with a nanofluid is the scope of the present study. The cavity considered is a square enclosure having a lower temperature sliding lid at the top, a differentially higher temperature wavy wall at the bottom, and two thermally insulated walls on the sides. The nanofluid medium used is a water-based nanofluid, Al_2O_3-water with various volume fractions of its solid. To carry out the numerical simulations, the developed governing equations are determined in terms of the stream function-vorticity formulation. The weighting function in the weak formulation of the governing equations is taken as unity, and the field variables are approximated using the MLS interpolation. Capability as well as adaptability of the proposed meshless technique is ascertained by close comparisons of the illustrated results obtained through the mesh-free method with those obtained through a traditional method already existing in the literature. Effective viscosity and thermal conductivity of the solid-liquid mixture are determined using the Brinkman and Maxwell models, respectively. A parametric study conducted through the present method to gain insight into the nanofluid convective heat transfer performance shows rational and deducible results. The study reveals that, distributions of the local Nusselt number along the wavy hot wall closely follow the pattern of the wall's geometry for different Richardson numbers and the nanoparticles volume fractions considered.

Keywords: MLPG, nanofluid, mixed convection, meshless, lid-driven, wavy cavity, numerical method

[1] Department of Mechanical Engineering, University of Kashan, Kashan, Iran
[2] Department of Mechanical Engineering, Science and Research Branch, Islamic Azad University, Tehran, Iran
[3] Department of Mechanical Engineering, University of Kashan, Kashan, Iran

Nomenclature

c_p	specific heat
Pr	Prandtl number
g	gravitational acceleration
Re	Reynolds number
Gr	Grashof number
Ri	Richardson number
H	cavity height
S	collection of nodal points
h	heat transfer coefficient
$t-n$	coordinates
k	thermal conductivity
T	temperature
L	cavity width
U,V	dimensionless velocity components
N	MLS interpolation function
$\mathbf{x}$	Cartesian coordinates vector
n	normal vector
x-y	Cartesian coordinates
n_k	number of interpolation nodes
$X-Y$	dimensionless Cartesian coordinates
Nu	Nusselt number
W	test function

Greek Symbols

α	thermal diffusivity
Ω	dimensionless vorticity
β	thermal expansion coefficient
Ω_I	control volume
Γ	boundary
ω	vorticity
Γ_h,Γ_I	boundary segment
Ψ	dimensionless stream function
μ	dynamic viscosity
Φ	stream function
ν	kinematic viscosity
θ	dimensionless temperature
ρ	density

φ nanoparticles volume fraction
Ω domain

Subscripts

c cold
in inside
eff effective
l cavity lid
f base fluid
nf nanofluid
h hot
s solid particle
I point or control volume number
w wall

Superscripts

$\hat{}$ nodal value
– approximation, average

1 Introduction

As a remedy to overcome the complexities regarding the mesh generation in conventional numerical techniques, the finite volume and finite element methods, some different mesh-free approaches have been introduced [Atluri and shen (2002); Liu (2003); Atluri (2004)]. In the earlier mesh-free techniques [Nayroles, Touzot and Villon (1992); Belytschko, Krongauz, Organ, Flemming and Krysl (1996); Lu, Belytschko and Gu (1994); Zhu and Atluri (1998)], an auxiliary grid was required to evaluate the integrals resulting from applying the Galerkin method to the differential equations. Hence, these methods could not be considered totally meshless. Subsequently, two truly meshless techniques- the meshless local boundary equation (MLBE) method, and the meshless local Petrov-Galerkin (MLPG) method- were proposed by Zhu, Zhang and Atluri [1998], and Atluri and Zhu [1998, 2000], respectively. To obtain the discretized equations in the latter scheme, the shape functions from the moving least squares (MLS) interpolations were employed in a local weak form of the differential equations over a local sub-domain. Atluri's

book [2004] presents a recent comprehensive review of the MLPG methods with emphasis on the solid mechanics applications.

Many efforts have been made to implement the MLPG method on the fluid flow and convection heat transfer analysis. Lin and Atluri [2000, 2001] applied the newly-developed MLPG method to the solutions of the convection-diffusion and the Navier-Stokes (N-S) equations. They modified the local weak forms to overcome the so-called Babuska-Brezzi conditions while solving the primitive variables from of the N-S equations. Moreover, they presented different upwinding scheme in order to obtain stabilized solutions under high Peclet (Pe) and Reynolds (Re) numbers. Liu [2003] investigated the performance of the MLPG method for simulating the buoyancy-driven heat transfer in a differentially-heated square cavity filled with air for Rayleigh numbers up to 10^5. His results showed that the MLPG method is more accurate than the finite difference method (FDM) using the same uniform nodal distributions. Arefmanesh, Najafi and Abdi [2005] applied a variation of the MLPG method with unity as the test function to the convection-diffusion and the potential flow equations. Comparisons of their results with the analytical solution for the convection-diffusion equation in a square domain demonstrated the high accuracy of their proposed method.

Arefmanesh, Najafi and Abdi [2008] used a variation of the MLPG method with unity test function to solve a number of non-isothermal fluid flow problems. They employed the stream function-vorticity formulation to solve different test cases such as a non-isothermal lid-driven cavity flow with an inlet and an outlet. Haji Mohammadi [2008] applied the MLPG method to simulate the incompressible viscous fluid flow. He formulated his considered cases in terms of the stream function-vorticity, and employed the radial basis function interpolations in his approach. Through introducing a new upwinding scheme, he obtained stabilized solutions for a square lid-driven cavity flow for Reynolds numbers up to 10^4. Dehghan and Mirzaei [2009] used the MLPG method for the unsteady magnetohydrodynamic flow through a pipe of rectangular cross section. They approximated the field variables by the MLS scheme, and employed unity as the test function in the local weak form. They concluded that the employed MLPG method was quite efficient and more flexible compared to the boundary element method. In another recent work, Avila and Atluri [2009] solved the unsteady two-dimensional N-S equations written in terms of the primitive variables using the MLPG method coupled with a fully implicit pressure correction approach. They solved the transient laminar flow field in a domain wherein certain surfaces had, a sliding motion, a harmonic motion, and an undulatory movement. They concluded in their work that the MLPG method coupled with a fully implicit pressure-correction algorithm was a viable alternative for the solution of fluid flow problems, particularly for those characterized

by non-steady fluid motion around flexible bodies with undulatory or contraction-expansion types of movements. Very recently, Wu, Tao, Shen and Zhu [2010] extended the MLPG method to solve the incompressible fluid flow problems using the primitive variables approach. They employed the streamline upwind Petrov-Galerkin (SUPG) method to obtain stabilized solution in convection-dominated problems, and applied the pressure-stabilizing Petrov-Galerkin method to satisfy the Babuska-Brezzi conditions. Their results showed that the method was stable, and resulted in converged solutions at high Reynolds numbers. Finally, in another study by Arefmanesh, Najafi and Nikfar [2010], the MLPG method was extended to investigate natural convection heat transfer in cavities with differentially-heated wavy side walls. Using the stream function-vorticity formulation and MLS interpolations, the analysis focused on the effects of the dimensionless amplitudes, wall's number of undulations, and Rayleigh number on the natural convection heat transfer within the considered enclosures. Their results showed a total validity and feasibility of the implemented code.

As far as using nanofluids in mixed convection analysis is concerned, only conventional methods, and nothing in application of mesh-free methods are reported. The behavior of nanofluids inside a two-sided lid-driven differentially-heated square cavity was investigated using the finite volume approach by Tiwari and Das [2007]. Copper-water nanofluid was used, and a model was developed to analyze the nanofluid behavior taking into account the solid volume fraction. The study concluded that both the Richardson number and the direction of the moving walls affect the fluid flow and heat transfer in the cavity. Ghasemi and Aminossadati [2010] studied mixed convection in a lid-driven triangular enclosure filled with an Al_2O_3-water nanofluid. Two different cases of upward and downward left sliding wall were considered. In their study, the power law profile approximation and the SIMPLE algorithm were used. The effects of the Richardson number, solid volume fraction, and direction of the sliding wall motion on the fluid flow, temperature fields, and heat transfer rate were examined. The results showed that the addition of Al_2O_3 nanoparticles enhanced the heat transfer rate for all values of the Richardson number, and for each direction of the sliding wall motion. A numerical investigation of laminar mixed convection using a Copper-water nanofluid in a square lid-driven cavity was executed by Talebi, Mahmoudi and Shahi [2010]. The conventional finite volume approach was used in this study. The horizontally moving top lid was insulated while the vertical walls were kept at constant, but different temperatures. The thermal conductivity and effective viscosity of the nanofluid were calculated using the Patel and Brinkman models, respectively. The study was carried out for Ra = 10^4-10^6, Re = 1-100, and for a range of the solid volume fraction from 0 to 0.05. The study showed that at a fixed Reynolds number, the solid concentration

affects the flow pattern and the thermal behavior of the nanofluid. The finite volume method using the SIMPLE algorithm was employed by Shahi, Mahmoudi and Talebi [2010] to solve the governing equations in another mixed convection heat transfer through a copper-water nanofluid. A square cavity with an inlet and an outlet ports was considered for which the convection effect was attained by heating from a constant flux heat source located at the bottom wall, and cooling from the injected flow. The Patel and Brinkman models were utilized to calculate the thermal conductivity and effective viscosity of the nanofluid, respectively. They concluded in this work that an increase in solid concentration leads to increase the average Nusselt number at the heat source surface and to decrease the average bulk temperature.

Among other recent works on mixed convection using nanofluids, is a study by Mansour, Mohamed, Abd-Elaziz and Ahmed [2010]. The heat transfer in a square lid-driven cavity partially heated from below, and filled with water and various volume fractions of Cu, Ag, Al_2O_3, and TiO_2 was investigated using the finite difference method. The effects of the Reynolds number, solid volume fraction, different values of the heat source length, and locations of the heat source on the streamlines and isotherms contours, and the local and average Nusselt numbers along the heat source were considered. The study concluded that increasing the solid volume fraction leads to decreasing both the activity of the fluid motion, and the fluid temperature. Also, an increase in the length of the heat source leads to an increase in the flow intensity and fluid temperature, but a decrease in the corresponding average Nusselt number. Muthtamilselvan, Kandaswamy and Lee [2010] conducted a study to investigate the transport mechanism of mixed convection in a lid-driven enclosure filled with Copper-water nanofluid (Pr = 6.2). For the enclosure, the two vertical walls were insulated while the horizontal walls were kept at constant temperatures with the top surface moving at a constant speed. The finite volume method with a staggered grid arrangement and the SIMPLE algorithm were employed to solve the governing equations. The study concluded that both the aspect ratio and solid volume fraction affected the fluid flow and heat transfer in the enclosure. Also, the variation of the average Nusselt number was found to be linear with the solid volume fraction.

Lattice Boltzmann Method was applied to investigate the mixed convection flows utilizing nanofluids (Cu, CuO or Al_2O_3 with water) in a lid-driven cavity by Nemati, Farhadi, Sedighi, Fattahi and Darzi [2010]. The effective thermal conductivity and viscosity of the nanofluids were calculated by Chon and Brinkman models, respectively. The results of this study indicated that the effects of the solid volume fraction grow stronger sequentially for Al_2O_3, CuO and Cu. Also, the study showed that an increase of the Reynolds number leads to a decrease of the solid

concentration effect. Abu-Nada and Chamkha [2010] applied a second order accurate finite volume method to study a steady laminar mixed convection flow in a lid-driven inclined square enclosure filled with Al_2O_3-water nanofluid. The left and right walls of the enclosure were insulated while the bottom and top walls were maintained at constant temperatures with the hot top surface moving at a constant speed. The study found that significant heat transfer enhancement can be obtained due to the presence of nanoparticles, and that this can be accentuated by inclination of the cavity at moderate and high Richardson numbers.

A literature scan reveals that the MLPG method is yet to be extended to analyze the mixed convection heat transfer through nanofluids. The present study focuses on acquiring a numerical solution through implementation of the MLPG method on a two-dimensional laminar mixed convection heat transfer using a nanofluid within a lid-driven wavy wall cavity. The study embraces analysis of some pertinent parameters on the heat transfer characteristics and fluid flow mechanisms of the utilized nanofluid within the enclosure.

2 Problem Formulation

Mixed convection fluid flow and heat transfer within a lid-driven square cavity with a wavy bottom wall is simulated numerically using the MLPG method. As depicted in Fig. 1, the height and the width of the cavity are denoted H and L, respectively, with $H = L$. The left and the right walls of the cavity are insulated while the bottom wall of the enclosure, which is a wavy wall, is maintained at a constant temperature T_h, here referred to as "hot" temperature. The enclosure's top wall, which moves in its own plane from left to right with a constant speed u_l , is kept at a constant temperature T_c , here referred to as "cold" temperature, with a differential temperature difference between T_h and T_c, so that $T_h > T_c$. The cavity is filled with a nanofluid composed of a mixture of water and Al_2O_3 spherical nanoparticles. The nanoparticles are presumed to be in thermal equilibrium with the base fluid, water. Moreover, there is no slip between the nanoparticles and the base fluid. The thermophysical properties of the base fluid and the nanoparticles are presented in Table 1. The nanofluid properties are assumed to be constant with the exception of the density which varies according to the Boussinesq approximation [Bejan (2004)]. The geometry of the wavy surface analyzed in this study is described by $y = 0.025\,(1 - \cos(6x))$, where x and y here are the Cartesian coordinates as shown in Fig. 1.

The steady-state fluid flow and heat transfer in the cavity are governed by the continuity, momentum, and energy equations. The natural convection term is incorporated in the momentum equation by employing the Bousinesq approximation [Bejan (2004)]. In this study, the two-dimensional fluid flow problem is formulated

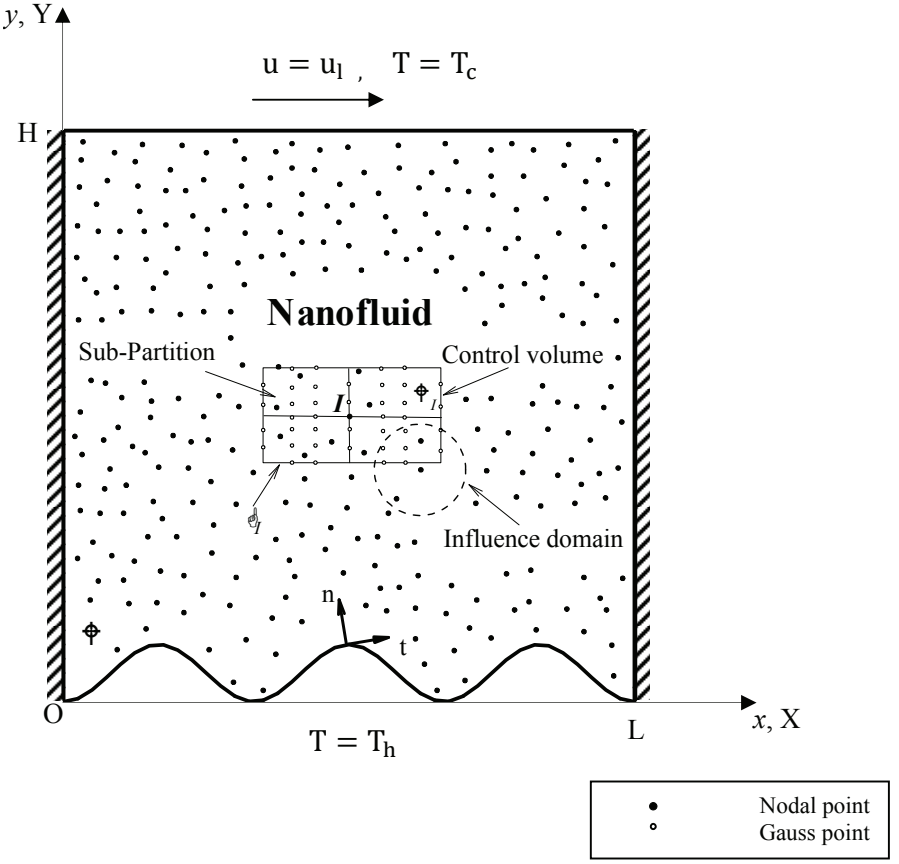

Figure 1: Lid-driven differentially-heated cavity, domain, boundary conditions, and a typical control volume

Table 1: Thermophysical properties of the base fluid and the nanoparticles [Ho, Chen and Li (2008)]

Property	Base fluid (water)	Nanoparticle (Al_2O_3)
c_p (J/kg K)	4179	765
ρ (kg/m^3)	997.1	3600
β (1/K)	2.1×10^{-4}	6.3×10^{-6}
μ (kg/m s)	8.91×10^{-4}	-
k (W/m K)	0.605	46

in terms of the stream function and vorticity.

To cast the governing equations into a dimensionless form, the following dimensionless variables are introduced:

$$X = \frac{x}{H}, \quad Y = \frac{y}{H}$$

$$U = \frac{u}{u_l}, \quad V = \frac{v}{u_l}, \quad \theta = \frac{T - T_c}{T_h - T_c} \tag{1}$$

$$\Psi = \frac{\Phi}{H u_l} \text{ and } \Omega = \frac{\omega H}{u_l}.$$

where u and v are the velocity component in the x and y-directions, respectively, Ψ is the stream function, and ω is the vorticity. Substituting the above dimensionless variables into the stream function, vorticity, and energy equations results in the following dimensionless form of the governing equations:

$$\frac{\partial^2 \Psi}{\partial X^2} + \frac{\partial^2 \Psi}{\partial Y^2} = -\Omega, \tag{2}$$

$$U\frac{\partial \Omega}{\partial X} + V\frac{\partial \Omega}{\partial Y} = \frac{\mu_{eff}}{\rho_{nf} \nu_f} \frac{1}{\mathrm{Re}} \left(\frac{\partial^2 \Omega}{\partial X^2} + \frac{\partial^2 \Omega}{\partial Y^2} \right) + \frac{\beta_{nf}}{\beta_f} \mathrm{Ri} \, \frac{\partial \theta}{\partial X} \tag{3}$$

and

$$U\frac{\partial \theta}{\partial X} + V\frac{\partial \theta}{\partial Y} = \frac{\alpha_{nf}}{\alpha_f} \frac{1}{\mathrm{Re}\,\mathrm{Pr}} \left(\frac{\partial^2 \theta}{\partial X^2} + \frac{\partial^2 \theta}{\partial Y^2} \right), \tag{4}$$

where ν_f, β_f, and α_f are the kinematic viscosity, thermal expansion coefficient, and thermal diffusivity of the base fluid, respectively. The subscripts *nf* and *eff* in the above equations refer to the words "nanofluid" and "effective", respectively. The Reynolds number, Re, the Richardson number, Ri, and the Prandtl number, Pr, are defined as

$$\mathrm{Re} = \frac{u_l H}{\nu_f}, \quad \mathrm{Ri} = \frac{g\beta_f (T_h - T_c) H}{u_l^2}, \quad \mathrm{Pr} = \frac{\nu_f}{\alpha_f} \tag{5}$$

Moreover, the Grashof number $\mathrm{Gr} = \mathrm{Ri} \times \mathrm{Re}^2$ is

$$\mathrm{Gr} = \frac{g\beta_f (T_h - T_c) H^3}{{\nu_f}^2} \tag{6}$$

The boundary conditions for the problem are specified and shown in Fig. 1. Writing the boundary conditions in terms of the stream function is straightforward. To write

the boundary condition for the vorticity, the following relation for the vorticity is employed for each wall of the cavity [Arefmanesh, Najafi and Nikfar (2010)]:

$$\Omega_w = \frac{2}{\triangle n^2}\left(\sqrt{U_w^2+V_w^2}\Delta n + \Psi_w - \Psi_{in}\right), \tag{7}$$

where n denotes normal direction (t is the perpendicular direction to n) to the wall, U_w and V_w are the components of the wall velocity in the X and Y-directions, respectively, and Ψ_w and Ψ_{in} are the values of the dimensionless stream function at a point inside the cavity next to the wall and on the wall, respectively.

2.1 Thermophysical Properties of the Nanofluid

The effective thermophysical properties of the nanofluid can be obtained from various formulas available in the literature. According to the Brinkman model [Brinkman (1952)], the effective viscosity of a dilute suspension of small rigid spherical particles in a fluid is given by

$$\mu_{eff} = \frac{\mu_f}{(1-\varphi)^{2.5}}, \tag{8}$$

where μ_f is the viscosity of the base fluid, and φ is the volume fraction of the nanoparticles.

The density, ρ_{nf}, the heat capacity, $(\rho c_p)_{nf}$, and the thermal expansion coefficient, $(\rho\beta)_{nf}$, of the nanofluid are obtained from the following formulas [Khanafer, Vafai and Lightstone (2003)]:

$$\rho_{nf} = (1-\varphi)\rho_f + \varphi\rho_s, \tag{9a}$$

$$(\rho c_p)_{nf} = (1-\varphi)(\rho c_p)_f + \varphi(\rho c_p)_s, \tag{9b}$$

$$(\rho\beta)_{nf} = (1-\varphi)(\rho\beta)_f + \varphi(\rho\beta)_s. \tag{9c}$$

The subscripts s and f in the above equations refer to the solid particles, and the base fluid, respectively.

The effective thermal conductivity of the solid-liquid mixture, k_{eff}, is evaluated from the Maxwell model [Khanafer, Vafai and Lightstone (2003)],

$$\frac{k_{eff}}{k_f} = \frac{(k_s+2k_f)-2\varphi(k_f-k_s)}{(k_s+2k_f)+\varphi(k_f-k_s)}, \tag{10}$$

where k_f, and k_s are thermal conductivities of the base fluid and the nanoparticles, respectively. Thermal diffusivity of the nanofluid is expressed as

$$\alpha_{nf} = \frac{k_{nf}}{(\rho c_p)_{nf}}. \tag{11}$$

The local Nusselt number based on the height of the cavity is evaluated from the following relation:

$$\mathrm{Nu} = \frac{h_{nf}\, H}{k_f}. \tag{12}$$

The heat transfer coefficient, h_{nf}, is obtained from

$$h_{nf} = \frac{q}{(T_h - T_c)}, \tag{13}$$

where, the wall heat flux per unit area, q, can be written as

$$q = -k_{nf} \frac{(T_h - T_c)}{H} \left.\frac{\partial \theta}{\partial n}\right|_{wall}. \tag{14}$$

Substituting Eqs. (13) and (14) into Eq. (12) yields the following relation for the local Nusselt number:

$$\mathrm{Nu} = -\frac{k_{nf}}{k_f} \left.\frac{\partial \theta}{\partial n}\right|_{wall}. \tag{15}$$

3 Numerical Procedure

In the present study, the governing equations are solved numerically by the MLPG method. To implement the method, an arbitrary collection of points is selected in the computational domain (Fig. 1). Subsequently, a control volume is generated around each of the points. A typical rectangular control volume Ω_I generated around point I is shown in Fig. 1.

As a first step in developing the discretized equations for the control volume Ω_I, the weak forms of the governing equations are to be obtained. This is accomplished by multiplying the stream function, vorticity, and energy equations by the test function W_I. Subsequently, the resulting equations are integrated over Ω_I. After performing the integration by parts, the weak forms of the stream function, vorticity, and energy equations for the control volume Ω_I are expressed, respectively, as:

$$-\int_{\Omega_I} \nabla W_I . \nabla \Psi d\Omega + \int_{\Gamma_I - \Gamma_I \cap \Gamma_h} W_I \frac{\partial \Psi}{\partial n} d\Gamma + \int_{\Gamma_I \cap \Gamma_h} W_I \frac{\partial \Psi}{\partial n} d\Gamma = -\int_{\Omega_I} W_I \Omega d\Omega, \tag{16}$$

$$\begin{aligned}\int_{\Omega_I} W_I \left(U\frac{\partial \Omega}{\partial X} + V\frac{\partial \Omega}{\partial Y}\right) d\Omega = \\ -\frac{\mu_{eff}}{\rho_{nf}\nu_f}\frac{1}{\mathrm{Re}}\int_{\Omega_I} \nabla W_I . \nabla \Omega d\Omega + \frac{\mu_{eff}}{\rho_{nf}\nu_f}\frac{1}{\mathrm{Re}}\int_{\Gamma_I - \Gamma_I \cap \Gamma_h} W_I \frac{\partial \Omega}{\partial n} d\Gamma \\ + \frac{\mu_{eff}}{\rho_{nf}\nu_f}\frac{1}{\mathrm{Re}}\int_{\Gamma_I \cap \Gamma_h} W_I \frac{\partial \Omega}{\partial n} d\Gamma + \frac{\beta_{nf}}{\beta_f}\mathrm{Ri}\int_{\Omega_I} W_I \frac{\partial \theta}{\partial X} d\Omega,\end{aligned} \tag{17}$$

$$\int_{\Omega_I} W_I \left(U\frac{\partial \theta}{\partial X} + V\frac{\partial \theta}{\partial Y} \right) d\Omega = -\frac{\alpha_{nf}}{\alpha_f}\frac{1}{\mathrm{Re\,Pr}}\int_{\Omega_I} \nabla W_I.\nabla\theta\, d\Omega + \frac{\alpha_{nf}}{\alpha_f}\frac{1}{\mathrm{Re\,Pr}}\int_{\Gamma_I-\Gamma_I\bigcap\Gamma_h} W_I\frac{\partial\theta}{\partial n}d\Gamma + \frac{\alpha_{nf}}{\alpha_f}\frac{1}{\mathrm{Re\,Pr}}\int_{\Gamma_I\bigcap\Gamma_h} W_I\frac{\partial\theta}{\partial n}d\Gamma \quad (18)$$

where Γ_h is the portion of the domain boundary for which a natural boundary condition is enforced. Here, Γ_I is the boundary of the control volume Ω_I , and $\Gamma_I \bigcap \Gamma_h$ represents the intersection of Γ_I with Γ_h.

Next, the integrals in Eqs. (16-18) are to be evaluated. The Gaussian quadrature is employed for this purpose. To perform the numerical integrations, the control volume Ω_I is divided into a number of sub-partitions (Fig. 1). The proper number of the Gauss points for the surface and the contour integrations in each sub-domain are selected. Subsequently, the field variables are approximated at each of the Gauss points using the MLS interpolations. Considering Ω_k as the interpolation domain for a typical Gauss point k, and $S_j, j = 1(1)\, n_k$, as a collection of n_k nodal points with coordinates $\mathbf{x}_j \in \Omega_k$ (whose influence domains cover the considered Gauss point), the unknown stream function, vorticity, and temperature fields are approximated within Ω_k, respectively, [Onate, Idelsohn, Zienkiewicz, Taylor (1996)] by

$$\overline{\Psi}^{(k)}(\mathbf{x}) = \int_{j=1}^{n_k} N_j^{(k)}(\mathbf{x})\hat{\Psi}_j, \quad (19a)$$

$$\overline{\Omega}^{(k)}(\mathbf{x}) = \int_{j=1}^{n_k} N_j^{(k)}(\mathbf{x})\hat{\Omega}_j, \quad (19b)$$

and

$$\overline{\theta}^{(k)}(\mathbf{x}) = \int_{j=1}^{n_k} N_j^{(k)}(\mathbf{x})\hat{\theta}_j \quad (19c)$$

where $\hat{\Psi}_j$, $\hat{\Omega}_j$, and $\hat{\theta}_j$ are the fictitious nodal values for the stream function, vorticity, and temperature, respectively. In Eqs. (19-a) through (19-c), $N_j^{(k)}(\mathbf{x})$, $j = 1(1)n_k$, are the MLS interpolation functions [Onate, Idelsohn, Zienkiewicz, Taylor (1996)].

Having obtained the weak formulations of the governing equations and the moving least-squares approximations of the field variables, the final step in the discretization process is to present the fully-discretized equations for a typical control volume Ω_I with the boundary Γ_I. The MLS interpolations for the stream function, vorticity, and temperature (Eqs. 19-a, b, and c) at a typical Gauss point k are substituted into

Eqs. (16-18). The resulting discretized equations are given by

$$\int_{j=1}^{n_k}\left(\int_{\Gamma_I-\Gamma_I\cap\Gamma_h} W_I\, N_{j,\ n}^{(k)}(\mathbf{x})\,d\Gamma\right)\hat{\Psi}_j = -\int_{j=1}^{n_k}\left(\int_{\Omega_I} W_I\, N_j^{(k)}(\mathbf{x})\,d\Omega\right)\hat{\Omega}_j$$
$$-\int_{\Gamma_I\cap\Gamma_h} W_I\frac{\partial\Psi}{\partial n}d\Gamma+\int_{j=1}^{n_k}\left(\int_{\Omega_I}\left(W_{I\ ,X}N_{j\ ,X}^{(k)}(\mathbf{x})+W_{I\ ,Y}N_{j\ ,Y}^{(k)}(\mathbf{x})\right)d\Omega\right)\hat{\Psi}_j, \quad (20)$$

$$\int_{j=1}^{n_k}\left[\int_{\Omega_I} W_I\left(UN_{j\ ,X}^{(k)}(\mathbf{x})+VN_{j\ ,Y}^{(k)}(\mathbf{x})\right)d\Omega-\frac{\mu_{eff}}{\rho_{nf}\nu_f}\frac{1}{\mathrm{Re}}\int_{\Gamma_I-\Gamma_I\cap\Gamma_h} W_I N_{j,\ n}^{(k)}(\mathbf{x})\,d\Gamma\right]\hat{\Omega}_j$$
$$+\frac{\mu_{eff}}{\rho_{nf}\nu_f}\frac{1}{\mathrm{Re}}\int_{j=1}^{n_k}\left(\int_{\Omega_I}\left(W_{I\ ,X}N_{j\ ,X}^{(k)}(\mathbf{x})+W_{I\ ,Y}N_{j\ ,Y}^{(k)}(\mathbf{x})\right)d\Omega\right)\hat{\Omega}_j$$
$$=\frac{\mu_{eff}}{\rho_{nf}\nu_f}\frac{1}{\mathrm{Re}}\int_{\Gamma_I\cap\Gamma_h} W_I\frac{\partial\Omega}{\partial n}d\Gamma+\frac{\beta_{nf}}{\beta_f}\mathrm{Ri}\int_{j=1}^{n_k}\left(\int_{\Omega_I} W_I N_{j\ ,X}^{(k)}(\mathbf{x})\,d\Omega\right)\hat{\theta}_j \quad (21)$$

and

$$\int_{j=1}^{n_k}\left[\int_{\Omega_I} W_I\left(UN_{j\ ,X}^{(k)}(\mathbf{x})+VN_{j\ ,Y}^{(k)}(\mathbf{x})\right)d\Omega-\frac{\alpha_{nf}}{\alpha_f}\frac{1}{\mathrm{Re\ Pr}}\int_{\Gamma_I-\Gamma_I\cap\Gamma_h} W_I\, N_{j,\ n}^{(k)}(\mathbf{x})\,d\Gamma\right]\hat{\theta}_j$$
$$+\frac{\alpha_{nf}}{\alpha_f}\frac{1}{\mathrm{Re\ Pr}}\int_{j=1}^{n_k}\left(\int_{\Omega_I}\left(W_{I\ ,X}N_{j,X}^{(k)}(\mathbf{x})+W_{I\ ,Y}N_{j,Y}^{(k)}(\mathbf{x})\right)d\Omega\right)\hat{\theta}_j$$
$$=\frac{\alpha_{nf}}{\alpha_f}\frac{1}{\mathrm{Re\ Pr}}\int_{\Gamma_I\cap\Gamma_h} W_I\frac{\partial\theta}{\partial n}d\Gamma. \quad (22)$$

The weighting function W_I is taken to be unity ($W_I = 1$) in the present study.

Similar discretized equations are obtained for all the Gauss points within the control volume Ω_I, and in turn, for all the control volumes of the domain. Assembling these equations for the control volumes and enforcing the essential boundary conditions by the direct interpolation method yield a set of algebraic equations for the stream function, vorticity, and temperature. Solving this system of the algebraic equations yields the unknown values of the field variables at the points.

4 Benchmarking of the Code

To validate the proposed developed scheme, a mixed convection simulation in a square cavity is carried out using the code. The results of the simulation are compared with the existing numerical results in the literature obtained using the FVM by Moallemi and Jang [1992].

Similar to the test case of Moallemi and Jang [1992], in the present study, the lid-driven mixed convection in a square cavity is simulated. The cavity comprises two

insulated side walls, a horizontally moving constant temperature cold wall at T_c , and a hot constant temperature bottom wall at T_h , with $T_h > T_c$. The motion of the top lid is from left to right with a constant speed of u_l. The cavity is filled with a fluid with Pr = 1.

Figure 2 shows the streamlines and the isotherms obtained by the MLPG simulation for Ri = 1 (Gr = 10^6, Re = 1000), and Pr = 1. The appropriate results presented by Moallemi and Jang [1992], for the exact same parameters, using the FVM are also shown in this figure. As it can be seen from Fig. 2, very good agreements exist between the streamlines and the isotherms obtained by the MLPG simulation and those of Moallemi and Jang [1992]. Comparisons between the local Nusselt numbers for the cold and the hot walls of the cavity obtained by the proposed MLPG method for Pr = 1, and the respective results of Moallemi and Jang [1992] which are given for Pr = 7.1, 1, 0.1, and 0.01 are presented in figure 3. As it is observed from this figure, excellent agreements exist between the two methods.

5 Results and Discussions

The proposed code is now applied to investigate the characteristics of the mixed convection heat transfer in the square cavity with a wavy bottom wall filled with the Al_2O_3-water nanofluid (Fig. 1). The calculations performed are for Gr = 10^4, for a range of Ri from 0.01 to 100, and three volume fractions of the nanoparticles, namely, 0.03, 0.06, and 0.1.

Figure 4 shows the streamlines inside the cavity for different Richardson number and volume fractions of the nanoparticles in comparison with the same cavity when filled with only the base fluid, water, (φ = 0). For Ri = 0.01, the fluid flow in the cavity is established by the shear action of the moving lid, and the buoyancy effect is not significant. A large primary clockwise eddy is generated inside the cavity as a result of the nanofluid moving next to the lid (Fig. 4-a). As the figure shows, a small counter-clockwise eddy referred to as the DSE (downstream eddy) develops in the bottom right corner of the cavity as a result of the stagnation pressure and frictional losses. Another smaller contour-clockwise eddy, called the USE (upstream eddy) is generated in the bottom left corner of the cavity as a result of the negative pressure gradient generate by the primary recirculating nanofluid as it deflects upward over the left vertical wall (Fig. 4-a). The negative pressure gradient is due to decreasing the horizontal velocity component and the corresponding increase of the pressure as the nanofluid close to the bottom of the cavity approaches the left vertical wall.

As it can be seen from Fig. 4, the effect of the natural convection on the fluid flow and heat transfer inside the cavity intensifies with increasing the Richardson number while keeping the volume fraction of the nanoparticles and the Grashof number

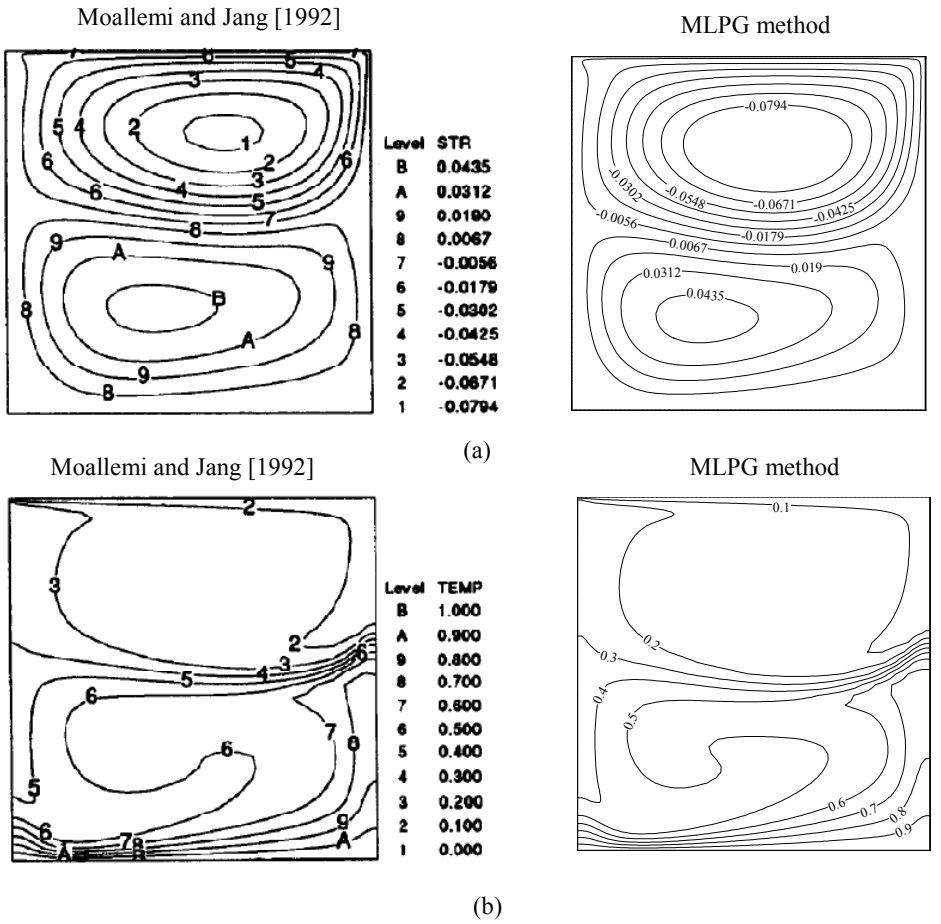

Figure 2: Streamlines and isotherms, comparison between the MLPG method and the FVM results by Moallemi and Jang [1992] for Ri = 1.0, (Gr = 10^6, Re =1000), Pr = 1.0 (a) streamlines (b) isotherms

constant. Consequently, the nanofluid adjacent to the hot wall of the cavity moves from the bottom right corner upwards enlarging the DSE, so that, it would occupy a good portion of the lower half of the cavity (Figs. 4-c and d). However, for Ri = 100, the lid-induced fluid flow is weak (Re = 10), hence the DSE disappears. The natural convection, in this case, assists the shear action of the moving lid resulting in a single clockwise eddy inside the cavity (Fig. 4-e).

As far as the volume fraction of the nanoparticles, Fig. 4 shows that the DSE diminishes in size and strength with increasing the volume fraction of the nanoparticles.

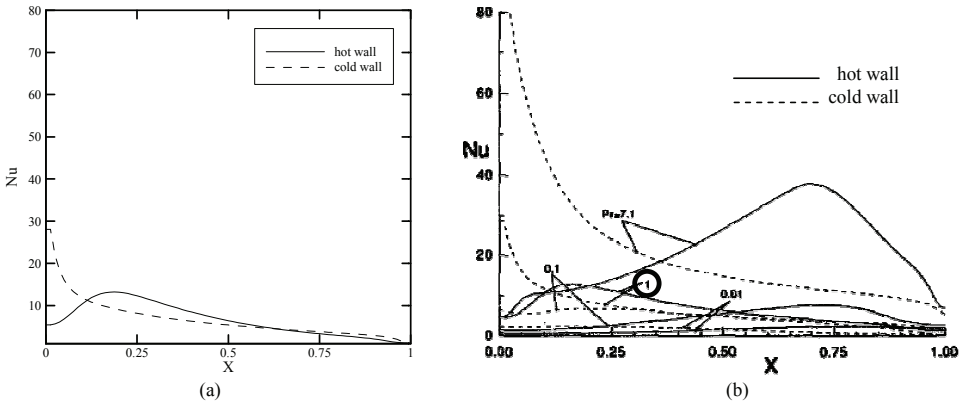

Figure 3: Local Nusselt numbers, comparison between the MLPG method and the FVM results by Moallemi and Jang [1992] for Ri = 1.0, (Gr = 10^6, Re =1000), Pr = 1.0 (a) MLPG method (b) Moallemi and Jang [1992]

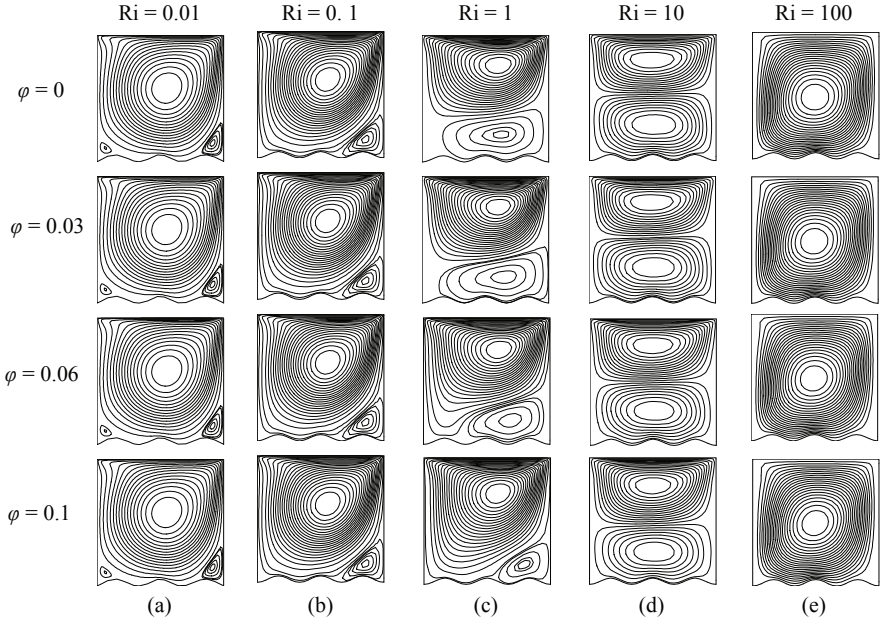

Figure 4: Streamlines for Al_2O_3-water nanofluid inside the cavity (Gr = 10^4)

This effect, which can be observed from Figs. 4-c and d for Ri = 1 and 10, respectively, is due to an increase in the effective viscosity of the nanofluid. This suppresses the natural convection, and diminishes the DSE for a constant Grashof number. Moreover, the primary recirculating eddy enlarges as a result of the diminishing DSE. For Ri = 0.01, the DSE, which is quite small, is due to the shear action of the moving lid, and, as such, it is not very sensitive to the volume fraction changes of the nanoparticles, as it can be seen in Fig. 4-a. In fact, for low Ri values, variations of the nanofluid viscosity do not have significant effects on the streamlines patterns (Figs. 4-a and b).

Figure 5 shows the isotherms inside the cavity for different Richardson numbers and volume fractions of the nanoparticles, with $\varphi = 0$ representing the base fluid, water only. For Ri = 0.01, the forced convection-dominated regime in Fig. 5-a is of the boundary layer type. This can be seen from the distinct thermal boundary layers formed along the top and bottom walls of the cavity. The relatively large core region of the cavity in this case is nearly isothermal. The isotherms at the bottom of the cavity follow the wavy pattern of the wall, i.e. they converge by moving towards the hills, and diverge by moving towards the valleys of the wavy wall. As the figure also indicates, the isotherms are less dense within the downstream and the upstream eddies (Fig. 5-a).

With increasing the Richardson number, while keeping the volume fraction of the nanoparticles constant, the DSE enlarges, and the thermal boundary layers thicken (Figs. 5-b and c). However, the core region of the primary eddy remains nearly isothermal. For Ri = 10, the primary and the downstream eddies are of comparable sizes, and as it is observed from Fig 5-d, a denser distribution of the isotherms exist close to the right side of the middle portion of the cavity. For Ri = 100, the isotherms in Fig. 5-e show a natural convection-dominated heat transfer regime for all the considered nanoparticles volume fractions. Therefore, the developed thermal boundary layers along the hot and the cold walls grow by moving towards the left and the right sides of the cavity, respectively. The core region in this case is nearly stratified.

Figures 6 and 7 show the variations of the dimensionless horizontal and vertical velocity components along the vertical and horizontal centerlines of the cavity, respectively, for different volume fractions of the nanoparticles ($\varphi = 0$ represents the base fluid, water). For Ri = 0.01 and 0.1, the fluid flow is established by the shear action of the moving upper lid. Hence, the upstream and downstream eddies are quite small, and the centerline velocity components are nearly independent of the volume fraction of the nanoparticles (Figs. 6-a and b, and 7-a and b). With increasing the Richardson number, Ri = 1 and 10, the DSE enlarges due to the enhancement of the natural convection. Hence, the horizontal centerline velocity

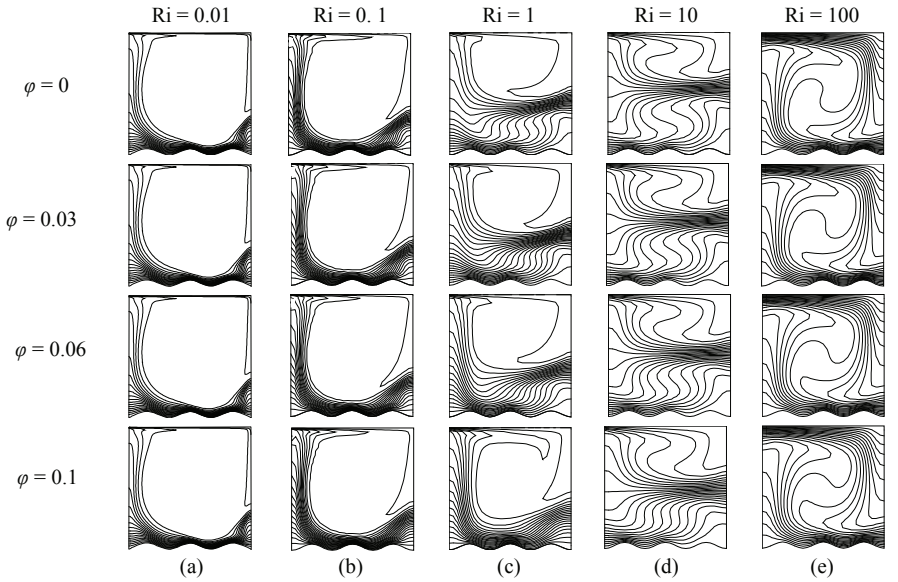

Figure 5: Isotherms for Al_2O_3-water nanofluid inside the cavity (Gr = 10^4)

component becomes positive in the vicinity of the bottom wavy wall, and its magnitude increases in this area with increasing the Richardson number (Figs. 6-c and d). For Ri = 100, the fluid flow is dominated by the natural convection which assists the relatively weak lid-induced forced convection. Hence, as Figs. 6-e and 7-e show, the centerline velocity components in some parts of the cavity can be much higher than the lid-velocity.

As far as the effects of the volume fraction of the nanoparticles on the horizontal and vertical centerline velocity components for moderate Richardson numbers (Ri = 1 and 10), in the area close to the bottom wavy wall, the horizontal centerline velocity component decreases with increasing the volume fraction as a result of suppression of the natural convection (Figs. 6-c and d). Also, as it is observed from Figs. 6-c and d, in the region from the center of the primary eddy to the vicinity where the two primary eddy and the DSE meet, the horizontal centerline velocity component in the primary eddy decreases with increasing the volume fraction of the nanoparticles as a result of the primary eddy enlargement. A reversed trend is observed in the upper portion of the DSE (from its center upwards) due to its shrinkage with increasing the volume fraction of the nanoparticles (Figs. 6-c and d). As it can be observed from Figs. 6-e and 7-e, for Ri = 100, increasing the vol-

ume fraction of the nanoparticles decreases the natural convection effects, and, in turn, reduces the centerline velocity component. For Ri = 1, the vertical centerline velocity component increases with increasing the volume fraction of the nanoparticles due to the shrinkage of the DSE (Fig. 7-c). However, for Ri = 10, as Fig 7-d shows the sign and the magnitude of the vertical centerline velocity component change drastically with the volume fraction of the nanoparticles depending on the relative sizes of the primary and the downstream eddies.

The local Nusselt number distributions along the hot and the cold walls of the cavity for different Richardson numbers and volume fractions of the nanofluid are shown in Figs. 8 and 9, respectively, with $\varphi = 0$ representing only water. As it is observed from Fig. 8, the Nusselt number distributions along the wavy bottom wall somehow follow the pattern of the wavy wall's geometry. The local Nusselt numbers maxima and minima occur in close proximity of the respective crests and troughs of the wavy wall, respectively. For Ri = 0.01 and 0.1, the maximum local Nusselt number occurs close to the middle portion of the wavy wall. Since the downstream and upstream eddies would result in decreasing the temperature gradient close to the right and the left bottom corners of the cavity (Figs. 8-a and b). For these Richardson numbers, the local Nusselt number increases with increasing the thermal conductivity of the nanofluid, and the shrinking downstream and upstream eddies (Figs. 8-a and b). Some similar observations could be made for the local Nusselt number for Ri = 1 as a result of the suppression of the DSE with increasing the volume fraction of the nanoparticles, (Fig. 8-c). Moreover, for Ri = 1, with decreasing the volume fraction of the nanoparticles, the DSE enlarges due to enhancement of the natural convection. This reduces the local Nusselt number along the entire length of the wavy wall (Fig. 8-c).

Fig. 8-d shows that, the location of the local Nusselt numbers maximum all shift to the left bottom corner of the cavity since as it was seen in Fig. 4-d, for Ri = 10, the DSE occupied a good lower portion of the cavity. For Ri = 100, the heat transfer inside the cavity occurs mainly through the natural convection, as the distribution of the isotherms in Fig. 5-e demonstrate. Hence, the maximum local Nusselt number occurs near to the crest closest to the right side wall (Fig. 8-e). Moreover, as Fig. 8-e shows the local Nusselt numbers drop sharply right after the closest crest to the right side wall due to the separation of the isotherms.

As the isotherms adjacent to the lid in Fig. 5 indicate, by moving from the left to the right along the lid of the cavity, the thermal boundary layer thickens, therefore, the local Nusselt number decreases (Fig. 9). It is also observed from Fig. 9, that by increasing the Richardson number, i.e. shifting the heat transfer to the natural convection-dominated regime, the local Nusselt number decreases. Moreover, the local Nusselt number, in general, increases with increasing the volume fraction of

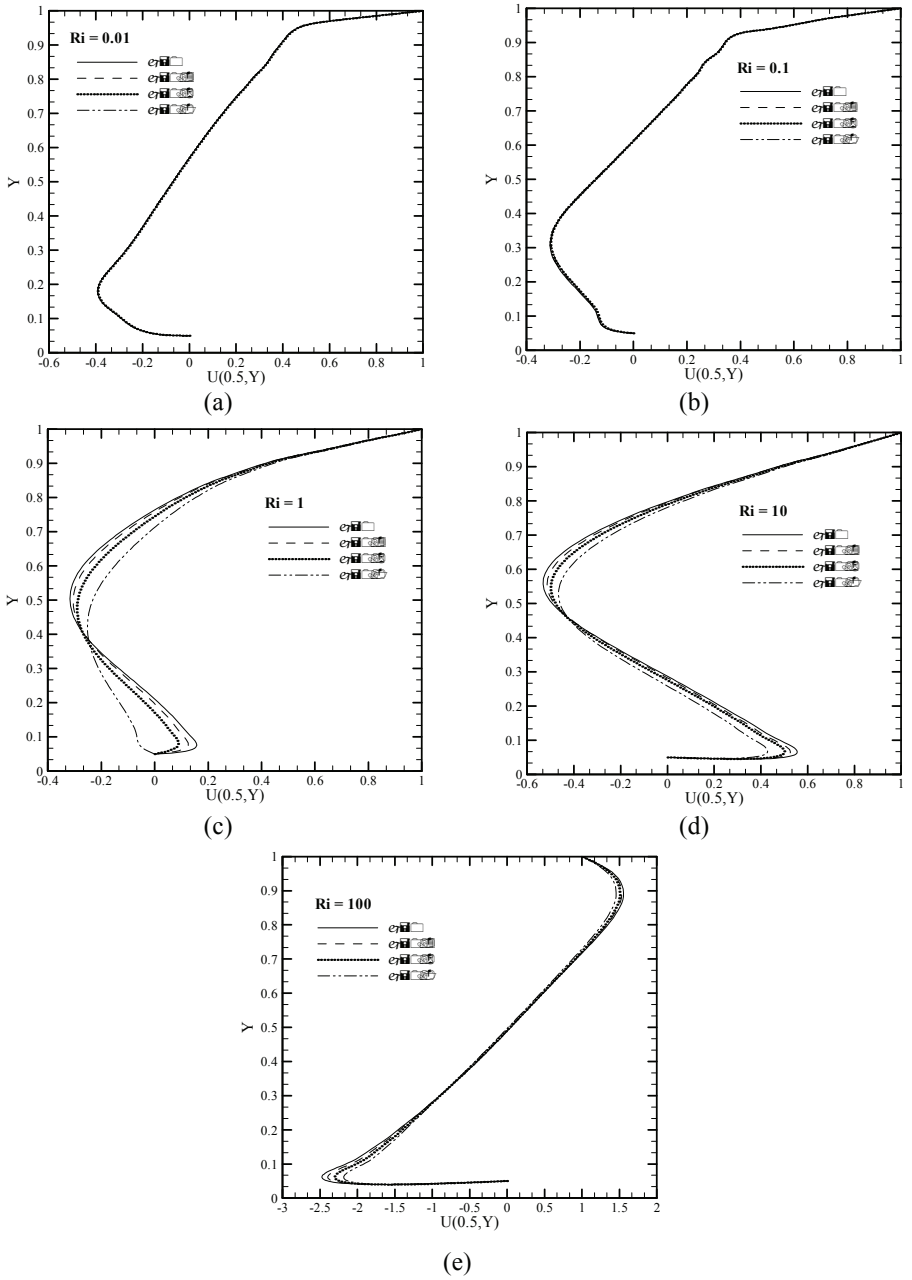

Figure 6: Variations of the dimensionless horizontal velocity component along the cavity vertical centerline for different nanoparticles volume fractions

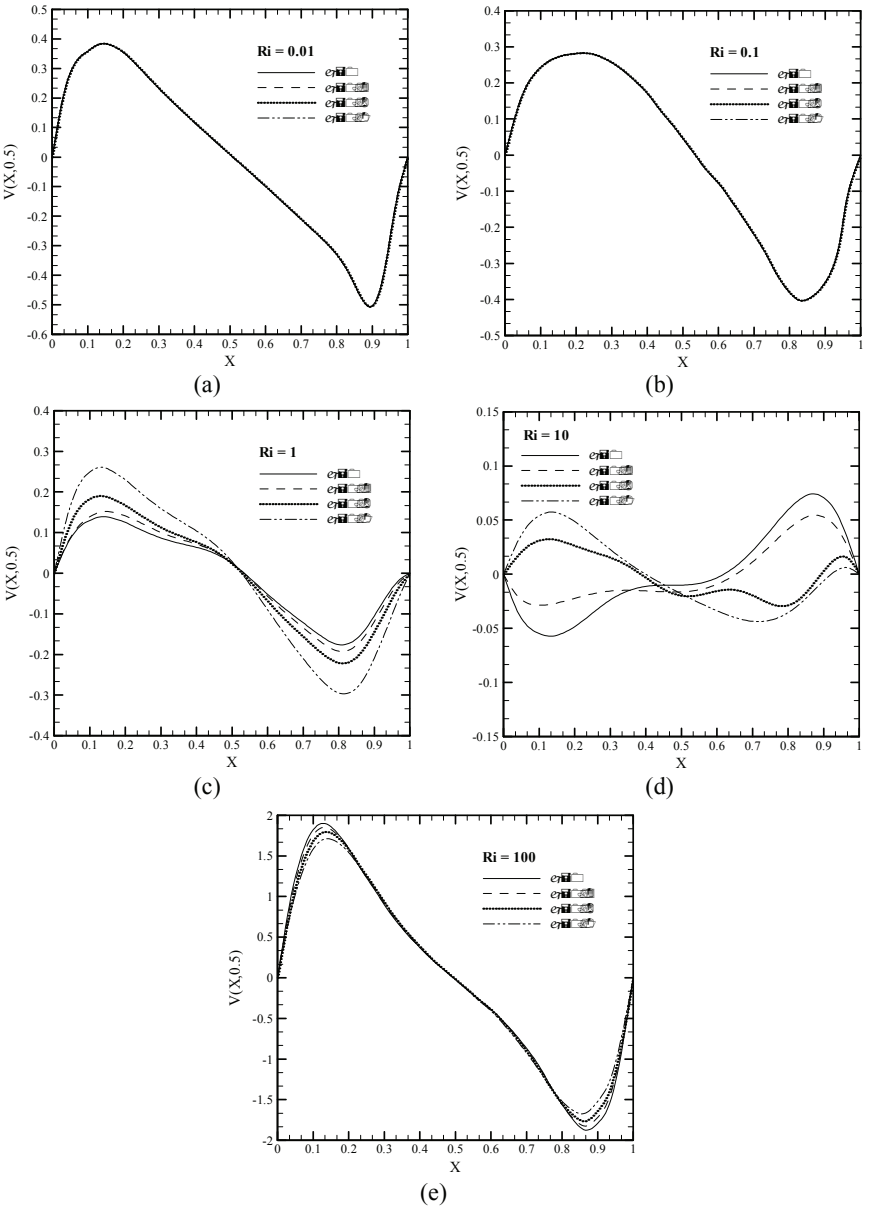

Figure 7: Variations of the dimensionless vertical velocity component along the cavity horizontal centerline for different nanoparticles volume fractions

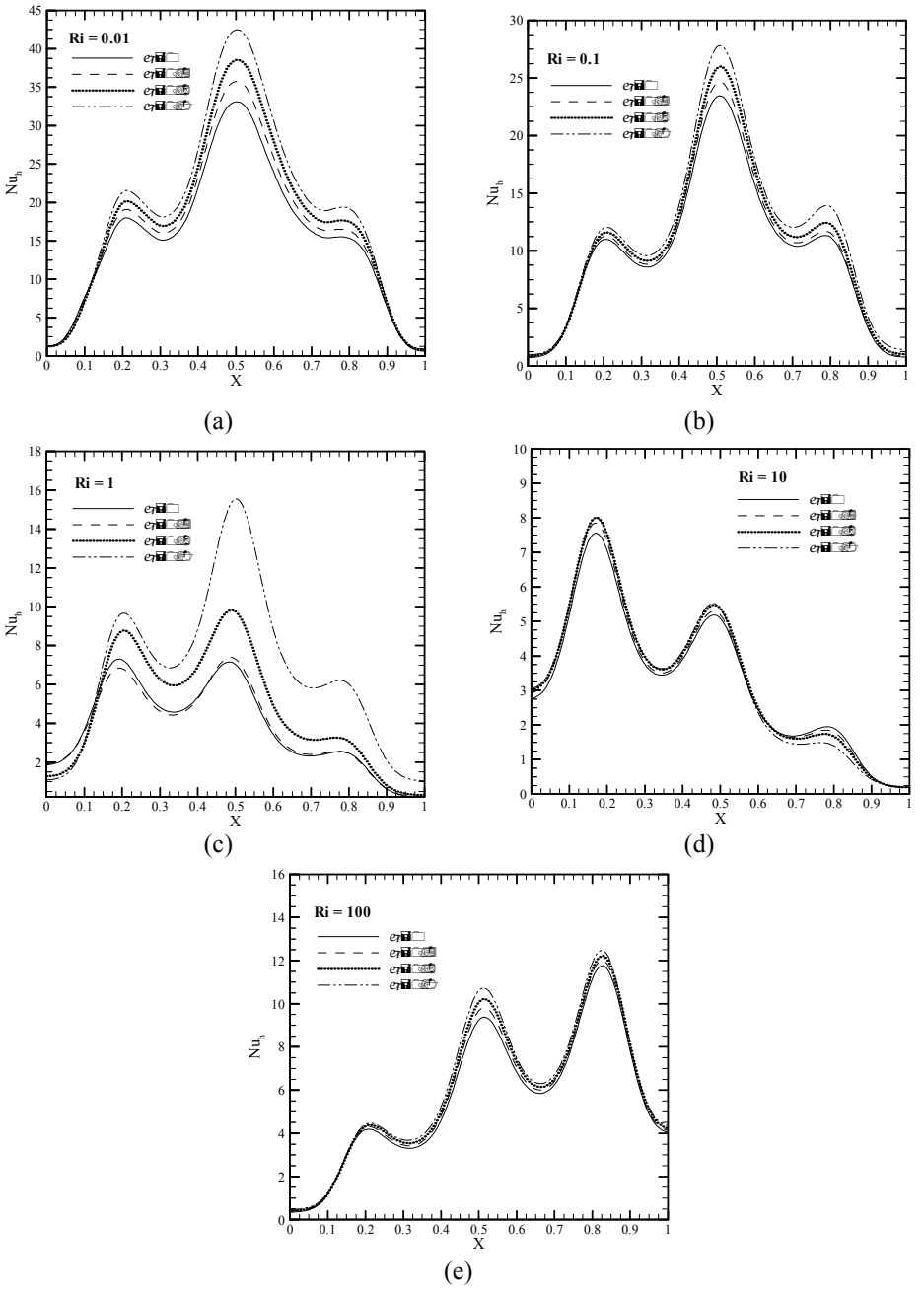

Figure 8: Variations of the local Nusselt number along the wavy wall for different nanoparticles volume fractions

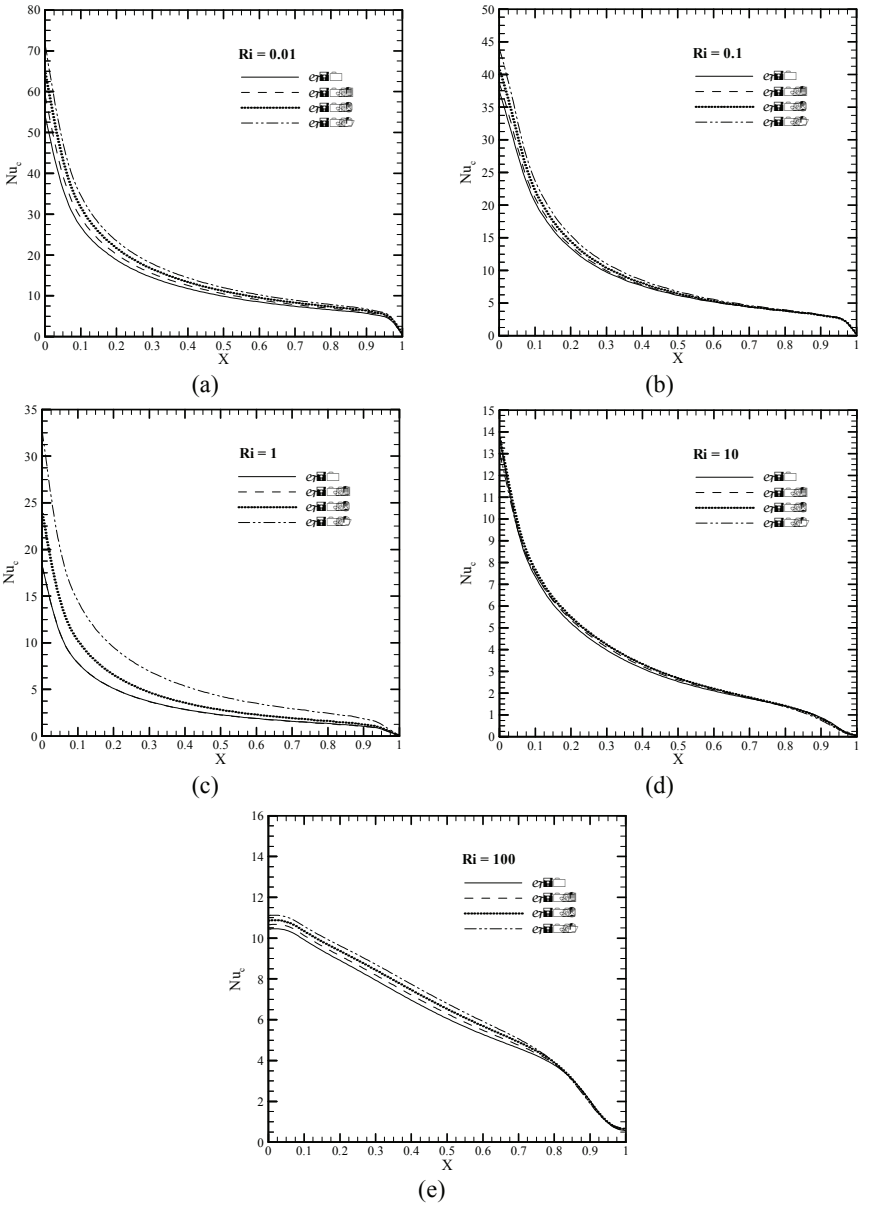

Figure 9: Variations of the local Nusselt number along the lid-driven wall for different nanoparticles volume fractions

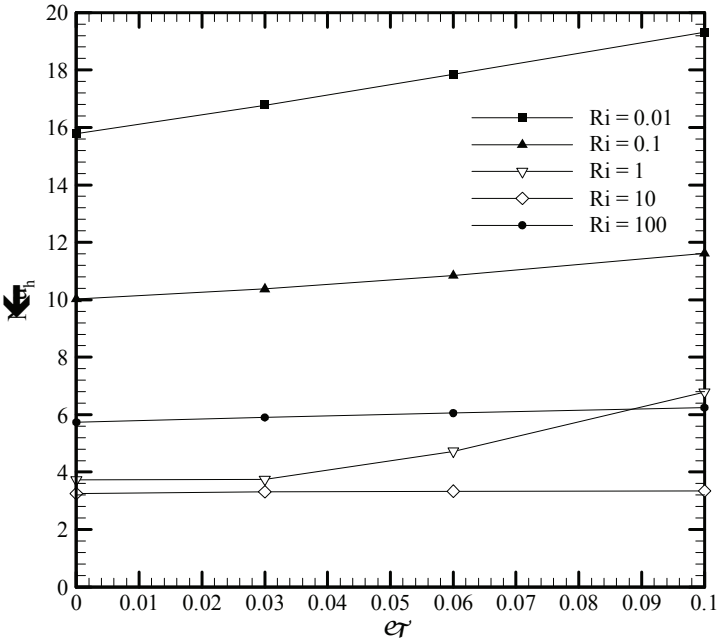

Figure 10: Variations of the average Nusselt number of the wavy wall with the volume fraction of the nanoparticles for different Richardson numbers

the nanoparticles as a result of increasing the thermal conductivity of the nanofluid and the shrinkage of the DSE (Fig. 9).

Figure 10 shows the variations of the average Nusselt number of the wavy hot wall with the volume fraction of the nanoparticles for different Richardson numbers. As it is observed from this figure, in general, heat transfer enhancement occurs with increasing the volume fraction of the nanoparticles. Also, as the figure shows, the enhancement of the heat transfer is quite substantial for lower Richardson numbers.

6 Conclusions

The applicability of the meshless local Petrov-Galerkin method to handle mixed convection heat transfer in a complex geometry containing a nanofluid is investigated. The validity of the meshless technique is demonstrated through the consenting results of the MLPG and the FVM.

Implications of some governing parameters such as nanoparticles volume fraction, and the Richardson number on the streamlines and isotherms contours, and on the

local and average Nusselt numbers were determined through the proposed method.

The local Nusselt number distribution picks up the waviness geometry of the wavy hot wall with the distribution maximum and minimum locations occurring at different spots of the hot wall length, depending on the value of the Richardson number. The average Nusselt number, however, in general, shows linearity with respect to the variation of the nanoparticles volume fraction for most of the implemented Richardson numbers.

Illustratively showing enhancement of convection heat transfer by increasing the nanoparticles volume fraction, in detail capturing all the respective corner eddies, and distinctively showing the effects of the natural versus forced convection heat transfer within the cavity demonstrate the competency of the present meshless technique for the application.

References

Abu-Nada E.; Chamkha A.J. (2010): Mixed convection flow in a lid-driven inclined square enclosure filled with a nanofluid. *European J. of Mechanics B/Fluids*, vol. 29, pp. 472-482.

Arefmanesh, A.; Najafi, M.; Abdi, H. (2005): A meshless local Petrov-Galerkin method for fluid dynamics and heat transfer applications. *J. of Fluids Eng*., vol. 127, pp. 647-655.

Arefmanesh, A.; Najafi, M.; Abdi, H. (2008): Meshless local Petrov-Galerkin method with unity test function for non-isothermal fluid flow. *CMES: Computer Modeling in Engineering & Sciences*. vol. 25, no. 1, pp. 9-23.

Arefmanesh, A.; Najafi, M.; Nikfar, M. (2010): Meshless local Petrov-Galerkin simulation of buoyancy-driven fluid flow and heat transfer in a cavity with wavy side walls. *CMES: Computer Modeling in Engineering & Sciences*, vol. 62, no. 2, pp. 113-149.

Atluri, S.N. (2004): The meshless method (MLPG) for domain and bie discretization. Tech. Science Press, USA.

Atluri, S.N.; Shen, S. (2002): The meshless local Petrov-Galerkin (MLPG) method. Tech. Science Press, USA.

Atluri, S.N.; Zhu, T. (1998): A new meshless local Petrov-Galerkin (MLPG) approach in computational mechanics. *Comput. Mech.*, vol.22, pp. 117-127.

Atluri, S.N.; Zhu, T. (1998): A new meshless local Petrov-Galerkin (MLPG) approach to nonlinear problems in computer modeling & simulation. *Computer Modeling & Simulation in Eng.*, vol. 3, pp.187-196.

Atluri, S.N.; Zhu, T. (2000): A new meshless local Petrov-Galerkin (MLPG) ap-

proach for solving problems in elasto-statics. *Comput. Mech.*, vol. 25, pp. 169-179.

Bejan, A., (2004): Convection heat transfer. 3rd ed., John Wiley & Sons, INC, Hoboken, New Jersey, USA.

Belytschko, T.; Krongauz, Y.; Organ, D.; Flemming, M.; Krysl, P. (1996): Meshless method: an overview and recent development. *Comput. Meth. Appl. Mech. Eng*., vol. 139, pp. 3-47.

Brinkman, H.C. (1952): The viscosity of concentrated suspensions and solutions. J. Chem. Phys. vol. 20, pp. 571-581.

Dehghan, M.; Mirzaei, D. (2009): Meshless Local Petrov–Galerkin (MLPG) method for the unsteady magnetohydrodynamic (MHD) flow through pipe with arbitrary wall conductivity. *Applied Numerical Mathematics*, vol.59, pp.1043-1058.

Ghasemi, B.; Aminossadati, S.M. (2010): Mixed convection in a lid-driven triangular enclosure filled with nanofluids. *Int. Communications in Heat and Mass Transfer*, vol. 37, pp. 1142-1148.

Ho, C.J.; Chen, M.W.; Li, Z.W. (2008): Numerical simulation of natural convection of nanofluid in a square enclosure: Effects due to uncertainties of viscosity and thermal conductivity. *Int. J. of Heat and Mass Transfer*, vol. 51, pp.4506-4516.

Khanafer, K.; Vafai, K.; Lightstone, M. (2003): Buoyancy-driven heat transfer enhancement in a two-dimensional enclosure utilizing nanofluids. *Int. J. of Heat and Mass Transfer,* vol. 46, pp. 3639-3653.

Lin, H.; Atluri, S.N. (2000): Meshless local Petrov-Galerkin (MLPG) method for convection-diffusion problems. *CMES: Computer Modeling in Engineering & Sciences*, vol. 1, no. 2, pp.45-60.

Lin, H.; Atluri, S.N. (2001): The meshless Local Petrov-Galerkin (MLPG) method for solving incompressible Navier-Stokes equations. *CMES: Computer Modeling in Engineering & Sciences*, vol. 1, no. 2, pp.117-142.

Liu, G.R. (2003): Meshfree method moving beyond the finite element method. CRC press, USA.

Lu, Y.Y.; Belytschko, T.; Gu, L. (1994): A new implementation of the element-free Galerkin method. *Comput. Meth. Appl. Mech. Eng.*, vol. 113, pp. 397-414.

Mansour, M.A.; Mohamed, R.A.; Abd-Elaziz M.M.; Ahmed S.E. (2010): Numerical simulation of mixed convection flows in a square lid-driven cavity partially heated from below using nanofluid. *Int. Communications in Heat and Mass Transfer,* In press.

Moallemi, M.K.; Jang, K.S. (1992)**:** Prandtl number effects on laminar mixed convection heat transfer in a lid-driven cavity. *J. Heat and Mass Transfer*. vol. 35, No. 8, pp. 1881-1892.

Muthtamilselvan, M.; Kandaswamy, P.; Lee, J. (2010): Heat transfer enhancement of Copper-water nanofluids in a lid–driven enclosure, *Commun Nonlinear Sci Numer Simulat,* vol. 15, pp. 1501-1510.

Nayroles, B.; Touzot, G.; Villon, P. (1992): Generalizing the FEM: Diffuse approximation and diffuse elements. *Comput. Mech*, vol. 10, pp. 307-318.

Nemati, H.; Farhadi, M.; Sedighi, K.; Fattahi, E.; Darzi A.A.R (2010): Lattice Boltzmann simulation of nanofluid in lid-driven cavity. *Int. Communications in Heat and Mass Transfer,* In press.

Onate, E.; Idelsohn, S.; Zienkiewicz, O.Z.; **Taylor, R.L.** (1996): A finite point method in computational mechanics: Applications to convective transport and fluid flow. *Int. J. Numer. Meth. Eng.*, vol.39, pp. 3839-3867.

Shahi, M.; Mahmoodi, A.H.; Talebi, F. (2010): Numerical study of mixed convective cooling in a square cavity ventilated and partially heated from the below utilizing nanofluid. *Int. Communications in Heat and Mass Transfer,* vol. 37, 201-213.

Talebi, F.; Mahmoodi, A.H.; Shahi, M. (2010): Numerical study of mixed convection flows in a square lid-driven cavity utilizing nanofluid*, Int. Communications in Heat and Mass Transfer*, vol. 37 pp. 79-90.

Tiwari, R.K.; Das M.K. (2007): Heat transfer augmentation in a two-sided lid-driven differentially heated square cavity utilizing nanofluids. *Int. J. Heat Mass Transfer*, vol. 50, pp. 2002-2018.

Wu, X.H.; Tao, W. Q.; Shen, S.P.; Zhu, X.W. (2010): A stabilized MLPG method for steady state incompressible fluid flow simulation. *J. of Comput. Physics,* vol. 229, pp. 8564-8577.

Zhu, T.; Atluri, S.N. (1998): A modified collocation & penalty formulation for enforcing the essential boundary conditions in the element free Galerkin method, *Comput. Mech.*, vol. 21, no. 3, pp. 211-222.

Zhu, T.; Zhang, J.D.; Atluri, S.N. (1998): Local boundary integral equation (LBIE) for solving nonlinear problems, *Comput. Mech.*, vol.22, pp. 174-186.